RSC Advances

PAPER

View Article Online
View Journal | View Issue

Cite this: *RSC Adv.*, 2022, **12**, 4311

Liquid cooling system for battery modules with boron nitride based thermal conductivity silicone grease

Xin Ge,[a] Youpeng Chen,*[b] Weidong Liu,[b] Guoqing Zhang,[a] Xinxi Li,*[a] Jianfang Ge[c] and Canbing Li[d]

Received 8th December 2021
Accepted 11th January 2022

DOI: 10.1039/d1ra08929c

rsc.li/rsc-advances

Heat-conductive silicone grease (HCSG), one of the most common composite thermal interface materials (TIMs) used in many advanced applications, is limited by its low thermal conductivity (TC). Different surface modification agents are required to improve the dispersion of TC additives and the interfacial compatibility with the silicone matrix. In this study, MQ silicone resin (MQ) was used to modify two kinds of self-made spherical boron nitrides (SBNs), with different particle sizes, using the sedimentation method. The amount of filler content allowed within the SBNs increased owing to the similar polarity of the MQ and the silicone matrix, and a HCSG with a TC of 1.22 W (m^{-1} K^{-1}) and a thermal resistance (TR) of 0.49 °C W^{-1} was obtained, respectively. In addition, the TC pathway was formed more easily with the 15 μm SBNs than with the 5 μm SBNs. In order to verify its potential application in battery thermal management, the HCSG was assembled on the surface of the liquid-cooling plate in the 18 650-battery module, and it was found that the maximum temperature of the battery module could be maintained below 42 °C, and the temperature difference could be controlled within 5 °C. Thus, with these excellent performances, the MQ silicone resin reported here, with respect to the assembly methods, will provide insights into the thermal management and energy storage fields.

1 Introduction

Lithium-ion batteries (LIBs) have been extensively employed in electric vehicles (EVs) owing to their high energy density, low self-discharge, and long cycling life.[1,2] To achieve a high energy density and driving range, the battery packs of EVs often contain several batteries. Owing to the compact construction, heat dissipation has become a huge problem. Studies have shown that batteries constantly generate significant heat during the charging and discharging process, reducing the battery performance and power life, and even causing deformation.[3,4] Thus, there is a need for an efficient battery thermal management system that enables the timely dissipation of heat. Air,[5–7] liquid,[8–10] and phase-change material (PCM) cooling[11–13] are the three principal thermal management technologies. However, owing to the technical level or properties of PCM defects, thermal interface materials (TIMs) are usually used to fill the microgaps in different shapes of liquid- or PCM-cooling systems to improve the heat transfer efficiency. Zheng *et al.*[14] designed dense aluminum cooling tubes installed around prismatic batteries, and the gap between the batteries and the cooling tubes was filled with TIMs. Liu *et al.*[15] prepared various heat-conductive silicone greases (HCSGs) by adding aluminum nitride, copper powder, and carbon fiber as thermal conductive additives and coating them between prismatic batteries and phase-change materials (PCMs) to control the temperature. Xiao[16] coated a commercial heat-conductive silicone grease (HCSG) between a soft package battery and homemade PCM to enhance the heat transfer efficiency. However, in all existing studies, TIMs were coated on the battery side. In long-term use, the HCSG may shift and contact the electrodes owing to its good fluidity, and the poor insulation results in a short circuit. Therefore, there is a need to develop an HCSG that provides a better thermal management solution in battery systems.

Boron nitride (BN), which exhibits a high thermal conductivity (TC) of 250–300 W (m^{-1} K^{-1}) and a low density, has been extensively studied as an ideal filler for TIMs.[17–19] However, BN cannot be well dispersed in the matrix owing to the surface inertia and poor interface compatibility with the polymer matrix. In addition, preliminary experiments have shown that flaky BN exhibits a thickening effect owing to its large specific surface area and other factors. To solve these problems, filler surface modification has been investigated.[20] To further improve the effect of surface modification, silicone resin has

[a]*School of Materials and Energy, Guangdong University of Technology, Guangzhou 510006, PR China. E-mail: pkdlxx@163.com*

[b]*Guangzhou Nanyang Polytechnic College, Guangzhou 510925, China. E-mail: chenyoupeng2016@163.com*

[c]*Zhongkai University of Agriculture and Engineering, Guangzhou 510230, Guangdong, PR China*

[d]*Department of Electrical Engineering, Shanghai Jiao Tong University, China*

recently been studied. Moreover, the sol–gel method has been widely used to introduce silicone resin on filler surfaces. Zhao[21] used SiO_2 to modify carbon nanotubes through the sol–gel method and compounded them with polyurethane, obtaining a material with a TC of 0.31 W (m^{-1} K^{-1}). Cui[22] also modified carbon nanotubes with SiO_2 using the sol–gel method and compounded them with epoxy resin. SiO_2 improved the interaction between the carbon nanotubes and the epoxy resin and increased the TC of the epoxy resin from 0.144 to 0.240 W (m^{-1} K^{-1}) at a fill content of 1 wt%. Ahn[23] modified the surface of BN particles with SiO_2, which increased the surface free energy of the particles and enhanced the interface adhesion with an epoxy dimethylsiloxane resin matrix. The author prepared a material with a TC of 3.1 W (m^{-1} K^{-1}), which is 24% higher than that of BN without modification. Kim[24] coated copper nanotubes with SiO_2 by introducing tetraethyl orthosilicate, which proved that an appropriate dosage of SiO_2 can enhance the TC of copper nanowire/epoxy terminated polydimethylsiloxane (PDMS) composites from 0.8 to 1.1 W (m^{-1} K^{-1}). MQ silicone resin (MQ), a polysiloxane with a chemical structure similar to that of SiO_2, consists of a mono-functional link ($R_3SiO_{1/2}$, M) and a quad-functional link ($SiO_{4/2}$, Q). MQ has been used to enhance the mechanical properties of silicone materials due to its good compatibility with silicone resin, enabling it to be used as a surface modification reagent and enhance the interface effect between fillers and the silicone matrix.

Owing to the MQ solubilizing in anhydrous ethanol rather than in water, a BN containing MQ fabricated using sedimentation instead of the complex "sol–gel" process has been proposed. Surface modification of MQ and its influence on the heat conductivity of HCSG has been explored. Furthermore, the prepared HCSG was coated between a battery module and a liquid-cooling plate to verify its availability.

2 Experimental

2.1 Materials

Platelet-like BN (1 μm) was purchased from Zibo Jingyi Ceramic Technology Co., Ltd, and the spherical BN (SBN) used was homemade. PDMS (500 and 10 mPa s) were provided by Guangzhou Suixin Chemical Co. Ltd. MQ was supplied by Guangzhou Delta Organic Silicon Technology Development Co. Ltd.

2.2 Preparation of the SBN

The method previously reported by Ren[25] was adopted herein. Spherical boron nitrides (SBNs) with different particle sizes (Fig. 1) were obtained under optimized manufacturing conditions using an air-flow spray dryer (SP-1500, Shanghai Shunyi Experimental Equipment Co. Ltd).

2.3 Surface modification of SBNs and preparation of HCSG

MQ and SBNs were dissolved in anhydrous ethanol and stirred to fully cover the SBNs with MQ. Deionized water was dripped slowly until no further precipitation occurred. The modified SBN powder (MQ@SBN) was filtered out and dried at 80 °C. Different weights of PDMS and MQ@SBN powder were fed into a planetary vacuum mixer (MT-0.75L, Guangzhou Tianze Machinery Equipment Co. LTD) and stirred for 3 h. The planetary vacuum mixer was maintained at −0.1 MPa and 75 °C (Fig. 2). Then, the HCSG was collected and aged for 1 d prior to testing.

2.4 Materials characterization

Fourier-transform infrared (FT-IR) spectroscopy was performed using a Spectrum100 spectrometer (PerkinElmer, USA) ranging from 4000 to 400 cm^{-1} at room temperature. The thermal stability of MQ@SBN was measured using thermogravimetric analysis (TGA, HCSGA2, Mettler Toledo, Switzerland). Scanning electron microscopy (SEM) was conducted using an ATC-SCUT scanning electron microscope (Carl Zeiss, Germany). The viscosity of the HCSG with different fillers was determined using a viscometer (NDJ-8S, Shanghai Jingtian electronic instrument Co. LTD) at 25 °C and 0.3 rpm. The TC and thermal resistance (TR) of the HCSG were measured using a TC-3000 TC meter (Xiaxi Electronic Technology Co., China) and a LW-9389 TR tester (Ruileng Technology Co., China), respectively. The heating diffusion was evaluated using a TiS10 FLUKE infrared thermal imager.

2.5 Preparation of the battery module and its experimental system

Fig. 3 shows a schematic diagram of the experimental system. Nine commercial 18 650 ternary lithium-ion power batteries with a capacity of 3200 mA h were connected in a 9P configuration (nine strings in parallel) using a laser-spot welding

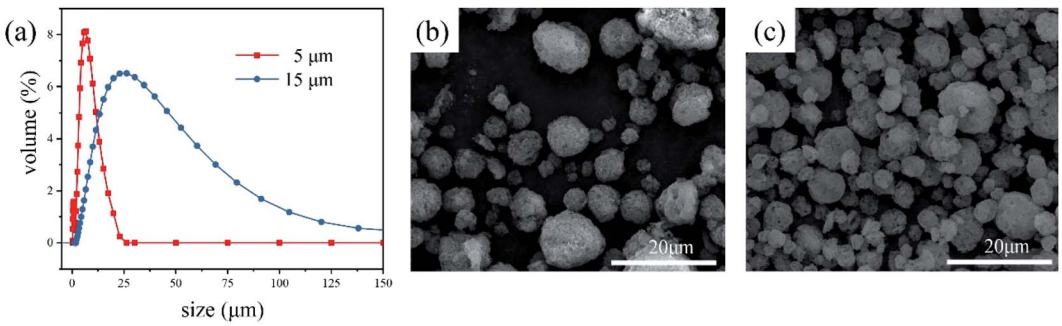

Fig. 1 Morphology and particle-size distribution of two specifications of SBNs.

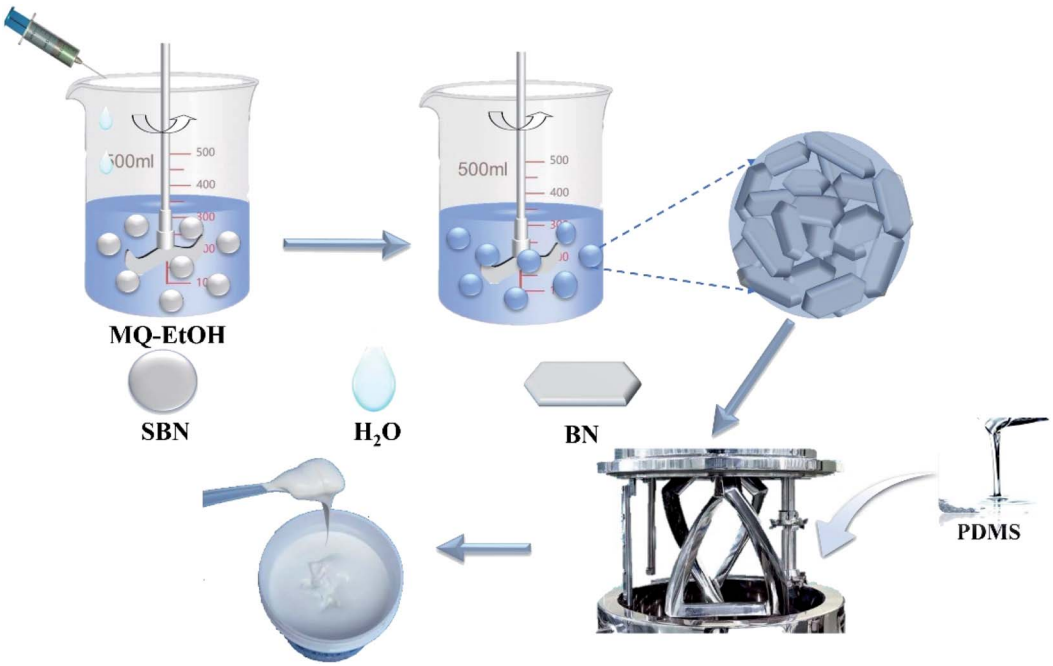

Fig. 2 Schematic diagram of the MQ@SBN preparation procedure.

machine. Finally, the battery module was charged/discharged using a BTS-5V30A-NTF battery-testing system (Shenzhen Neware Electronics Co. Ltd., China). Three T-type thermocouples were mounted on the center of the surface of the three cells in the battery module and connected to an Agilent 34970A data acquisition unit (Keysight Technologies, Inc.). The temperature of the oven was set as 30 °C and the charge–discharge parameters are shown in Table 1.

3 Results and discussion

3.1 Rheological behavior

Rheological behavior is a major concern in the practical processing of TIMs. The good rheological properties of TIMs make them easy to operate and they can be well fitted on a plane, which may result in a lower contact TR. Meanwhile, a weak thickening effect means that more additives can be filled into the matrix to achieve a high TC. Fig. 4a shows the viscosity of

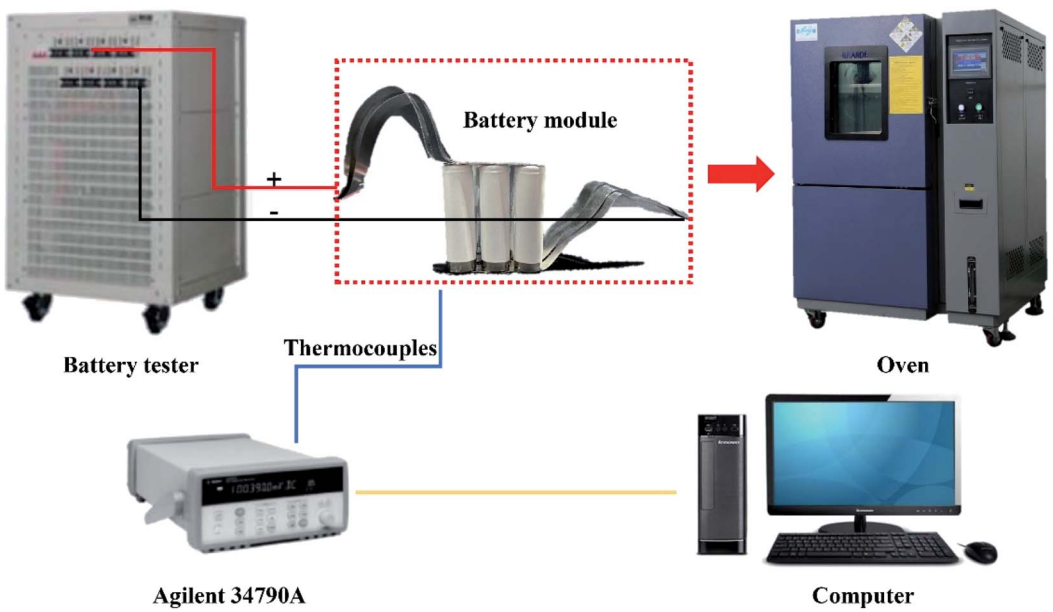

Fig. 3 Schematic diagram of the experimental setup.

Table 1 Charge–discharge parameters of the battery pack

Process	Time (min)	Current (A)	Cut-off voltage (V)
Rest	30	—	—
Constant current charge and constant voltage charge	—	28.8 (cut-off current of 2.0)	4.2
Constant current discharge	—	28.8	3.0
Rest	240	—	—

BN/PDMS and SBN/PDMS with various filler contents. Viscosity is a measure of the interior of a slurry system and it is sensitive to changes in the microstructure of the slurry system.[25] At a filler content of lower than 35 wt%, an increase in the filler content has little effect on the viscosity; it changes gradually. Once the filler content is above 35 wt%, the interior friction among the fillers and the interaction between the filler and polymer chains increases the viscosity.[26] Compared to the 1.0 μm platelet-like BN-filled mixture, the viscosity of the SBN-filled mixture is much lower at high filler content regions. Furthermore, larger SBNs contribute to the viscosity more than small SBNs. The reduction factor (η) of viscosity is introduced herein, which is defined as follows:

$$\eta = \frac{\mu_{1\mu m} - \mu}{\mu_{1\mu m}} \times 100\% \quad (1)$$

in which, μ and $\mu_{1\ \mu m}$ are the viscosities of the SBN-filled composite and the 1 μm BN/PDMS, respectively. Fig. 4b shows that when the filling content is 65 wt%, the viscosity of the 15 μm SBN/PDMS and 5 μm SBN/PDMS decreased by 47.9% and 29.4%, respectively, compared with that of the 1.0 μm BN/PDMS. The increase in viscosity is attributed to the interior friction. In addition, the probability of interactions and blockages occurring among the fillers increases because of the superior specific area of the platelet-like BN. Compared with the platelet-like BN, SBNs with a lower specific surface area have a reduced interfacial interaction with PDMS. This is the reason for the viscosity of the 5 μm SBN/PDMS being slightly higher than that of the 15 μm SBN/PDMS.

3.2 Surface treatment analysis

FT-IR analysis revealed that pristine SBN exhibits characteristic absorption bands at approximately 818 and 1378 cm^{-1}, which are attributed to the B–N–B and B–N bonds, indicating the transverse and in-plane vibrations, respectively (Fig. 5a).[27] The spectrum of MQ@SBN shows a band centered at 1087 cm^{-1}, ascribed to Si–O–Si asymmetric stretching. Meanwhile, the peaks at 1256 cm^{-1} (the variation of Si–CH_3) and 2955 and 850 cm^{-1} (the stretch of –CH_3) are evident of MQ.[28,29] The two weight loss steps in the curves during the decomposition of MQ (Fig. 5b) are, respectively, attributed to the evaporation of water (a byproduct of the thermal polycondensation reaction of the remanent hydroxyl groups) from room temperature to 250 °C and organic groups, including –CH_2–, CH_2=CH, –OCH_2CH_3 thermally decomposed from 250 to 700 °C. The final loss of SBN at 700 °C was 1.13%, including the binder and the absorption of a small amount of water. The weight loss of MQ@SBN was greater than that of the SBNs, reaching 3.17% at 700 °C, which indicates that MQ was effectively loaded on the SBNs. Elemental distribution analysis was employed to investigate the uniform modification of MQ by the sedimentation process. Fig. 5e–h show the B and N elements from the SBNs, and the Si element was from MQ. The hydroxyl groups on the surface of the SBNs and MQ provided the O elements. This shows that the sedimentation method could uniformly modify the SBNs with MQ.

The modification effect of MQ on SBN is attributed to the settling of the fillers in PDMS. Certain amounts of SBNs and MQ@SBN were fully suspended in the 10 mPa s PDMS using 30 s of ultrasonic treatment. As shown in Fig. 5i, the SBNs and MQ@SBN were dispersed uniformly in PDMS at the beginning. However, with time, the SBNs and MQ@SBN precipitated at different degrees owing to gravity. The presence of MQ slowed the precipitation of the SBNs, and this therefore layered slightly after 72 h. This is because MQ, as an organosilicon, has a molecular structure similar to that of PDMS, and the similar chemical polarity enhances the interaction between the SBNs and PDMS. Furthermore, as MQ has a cage-like structure, the chain-like PDMS can be "locked" inside, enabling SBN and PDMS to combine tightly.[30]

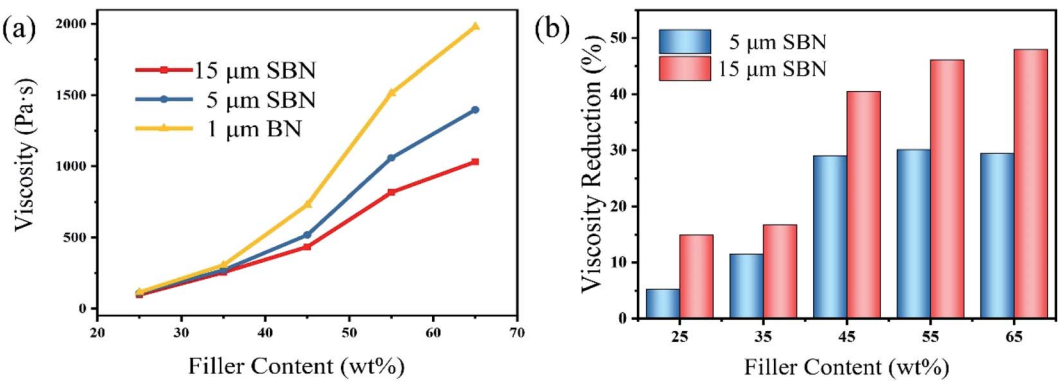

Fig. 4 (a) Viscosity of HCSG with different shapes and sizes of fillers. (b) Variation in the viscosity with filler content.

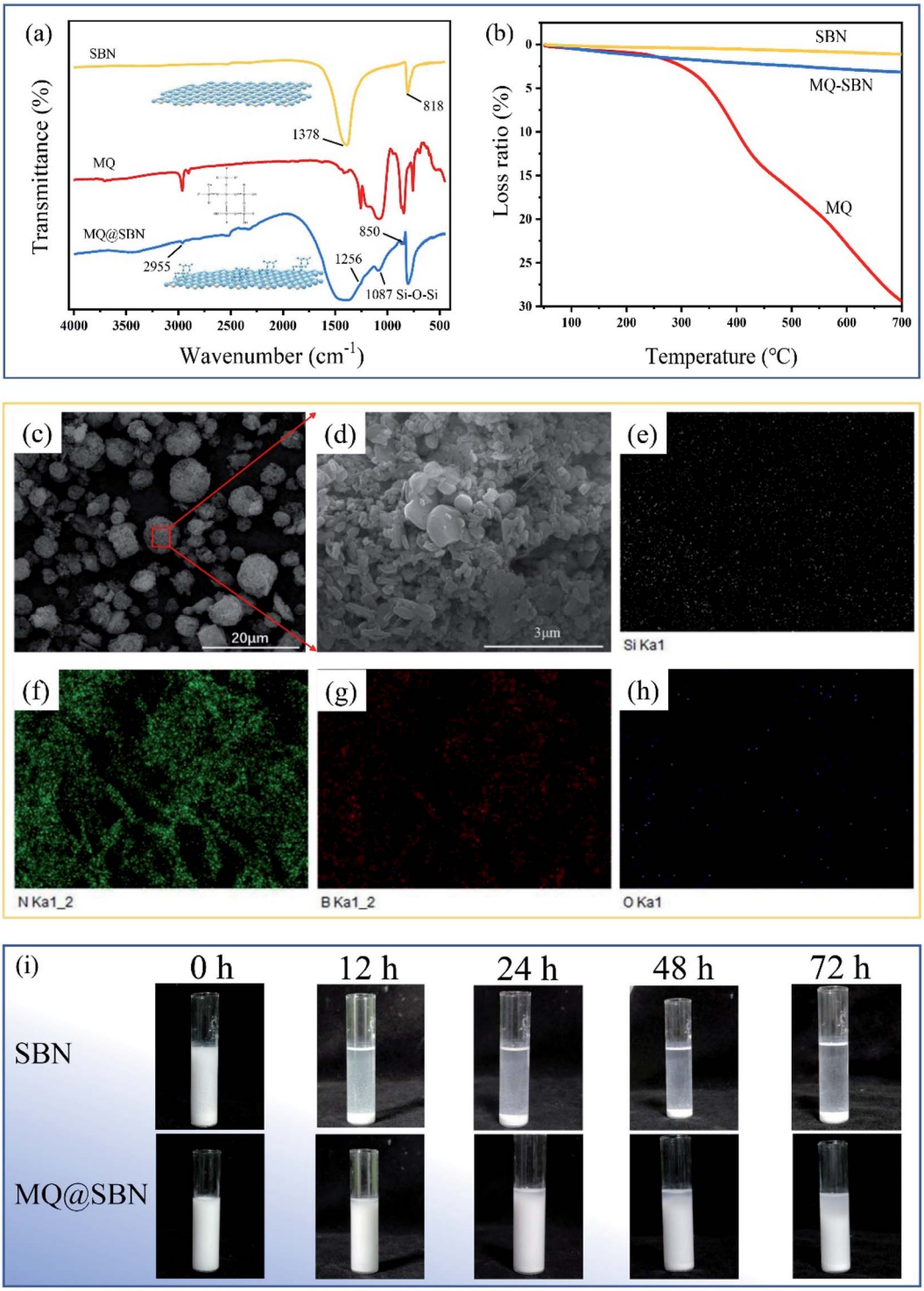

Fig. 5 (a) FT-IR spectrum of MQ@SBN. (b) TGA curves of SBN, MQ, and MQ@SBN. (c) and (d) SEM images of MQ@SBN and the elemental distribution of (e) Si; (f) N; (g) B; (h) O. (i) Settlement comparison of SBN and MQ@SBN.

3.3 Heat transfer performance

The matrix phonon propagation directly affects the TC of the materials, and the interfacial heat transfer between two dissimilar materials can be controlled by adjusting the phonon impedance of the two materials.[31] Previous studies have demonstrated that improving the phonon impedance matching between the polymer matrices and solid fillers can reduce the interface thermal resistance (ITR) and improve the TC of the polymer composites. [32–34] Surface modification of the fillers improves the phonon impedance matching. PDMS composites were fabricated with different weight ratios of MQ@SBN, and

the size of SBN was 15 μm. To determine the influence of the surface modification on the thermal transfer properties of HCSG, the TC of the fabricated MQ@SBN/PDMS was examined as a function of the MQ@SBN concentration, and the results are shown in Fig. 6a. The TC of the SBN/PDMS increased with an increase in the filler content. However, when the filler content of SBN was greater than 67 wt%, the TC of SBN/PDMS decreased because the filler content of SBN had reached the maximum. HCSG was so hardened that defects occurred inside SBN/PDMS, severely effecting its TC. In contrast, if the filler content of MQ@SBN was greater than 67 wt%, MQ@SBN/PDMS could still maintain a certain viscosity and wettability, and its TC showed an increasing trend. The thermal transport in SBN is mainly related to the phonon conduction. First, the MQ-layer chemical structure is similar to that of PDMS, and this makes it compatible with the PDMS matrix, enhancing the interfacial interaction between the matrix and SBN and decreasing the TR. Second, the MQ coating layer decreases the modulus mismatch between SBN and the PDMS matrix, reducing the ITR at the interface, thereby improving its phonon transmission.[21] Fig. 6b shows the relationship between the thermal transfer property and the MQ dosage. As an amorphous polymer, superfluous MQ with a low TC inevitably results in degradation. Therefore, it is necessary to explore the rational dosage. According to the similar compatibility principle, MQ may promote the interface compatibility between the fillers and the silicone matrix, enhancing the interaction between the fillers and the matrix, and improving the dispersion of the fillers.[35] With the same filler content, 1.0 wt% of MQ promoted TC, reaching 1.22 W (m^{-1} K^{-1}), compared to the 0.91 W (m^{-1} K^{-1}) of SBN/PDMS. However, above 1.0 wt% MQ, the TC decreased. This is because an increase in the portion of MQ, which has a lower TC than SBN, reduces the portion of the highly thermally conductive SBN, reducing the TC of the filler. The SEM morphological images (Fig. 6c–f) show that a layer with too much MQ does not form a uniformly composed and smooth layer but exhibits an aggregated rough surface. The rough surface forms a new ITR layer that increases the phonon scattering and reduces the TC.[22,24,36,37] Therefore, 1 wt% MQ was adopted for subsequent experiments.

To demonstrate the heat dissipation ability of the MQ@SBN/PDMS composite, a hot platform was utilized as the heat source to determine the heating transfer capacity during

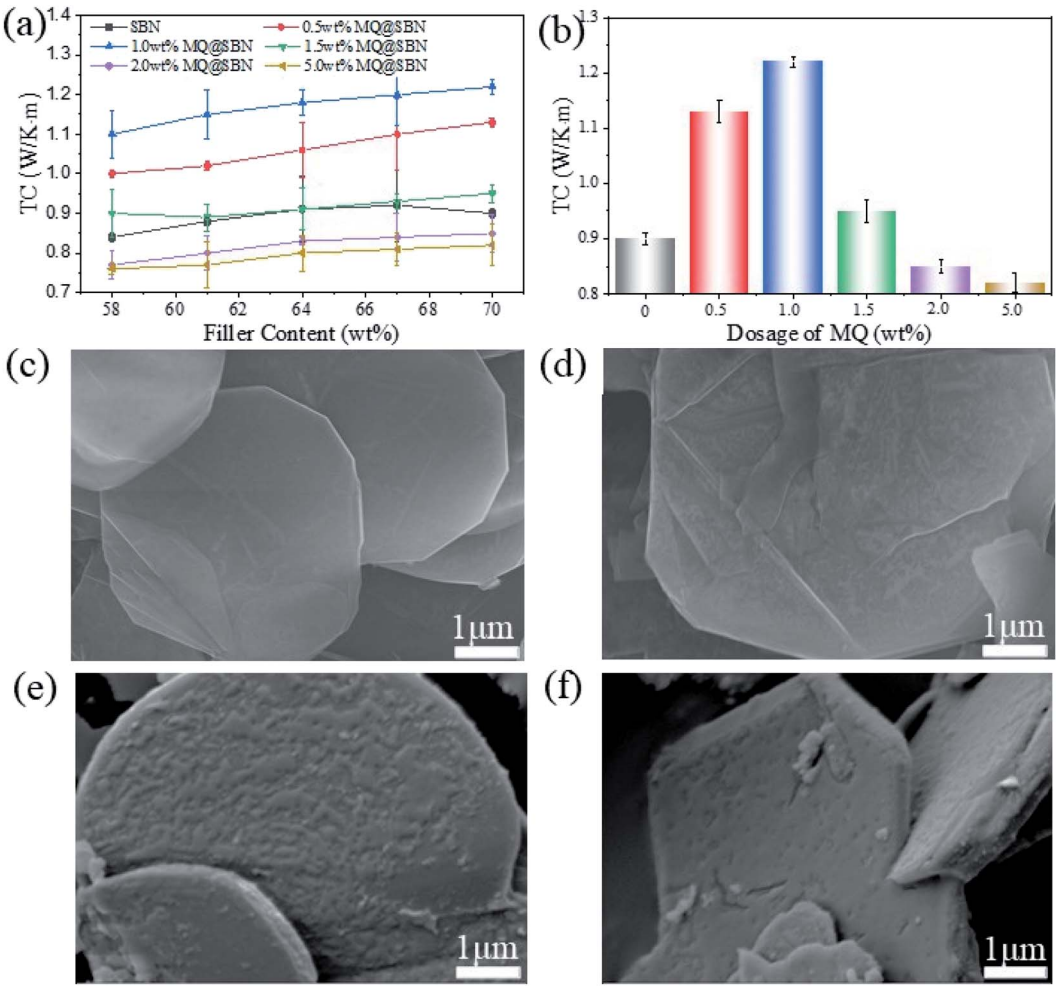

Fig. 6 (a) The influence of the MQ dosage on the TC. (b) The influence of the MQ dosage on the TC at a filler content of 70 wt%. Surface SEM images of (c) pure SBN, (d) 1.0 wt% MQ@SBN, (e) 2.0 wt% MQ@SBN, and (f) 5.0 wt% MQ@SBN.

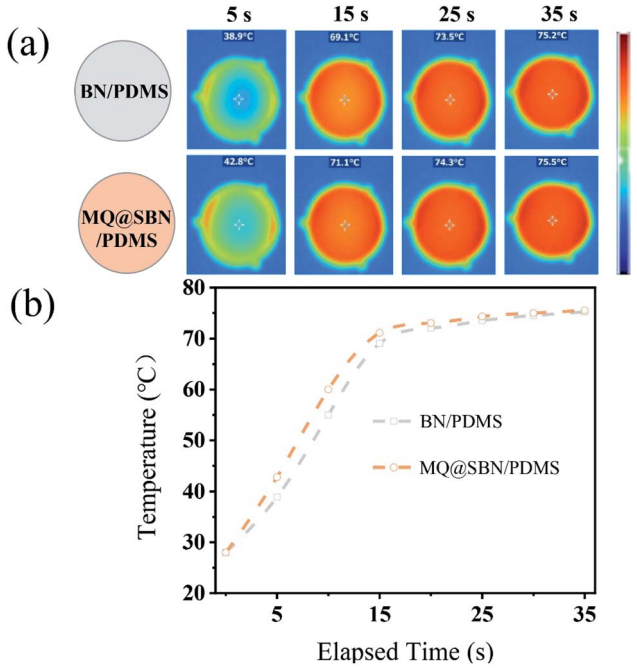

Fig. 7 (a) Infrared thermal images of the heating stage integrated with BN/PDMS and MQ@SBN/PDMS. (b) Corresponding surface temperature of the samples varying with the heating time.

the heating process. The thermography and temperature change of the platform were monitored and recorded every 5 s through infrared thermal images and are displayed in Fig. 7a. As MQ@SBN/PDMS possesses an optimized heat conduction network, it turned to a darker color more rapidly owing to its higher thermal conductivity. As shown in Fig. 7b, the MQ@SBN/PDMS composites exhibited a faster rate of temperature increase in the same working time, while the PDMS samples showed the slower rate of temperature change, therefore the MQ@SBN/PDMS could dissipate the accumulated heat in a timely and rapid manner. Thus, the composite materials exhibited significantly greater thermal conductivity than that of the pure PDMS, which as a thermally conductive material can be applied at the interface of composite materials to improve the thermal conductive performance. For these materials, the temperature of the platform surfaces were reduced by 15 °C, this can be attributed to the protective performance of the electrical devices during the operating process.[38]

As shown in Fig. 8a and b, the SBN/PDMS composites exhibited a higher TC than that of the platelet-like BN-filled composite for all filler contents. When the filler content was 58 wt%, the TC values for the three kinds of HCSG were 0.81, 0.95, and 1.11 W (m^{-1} K^{-1}). The spherical structure improved

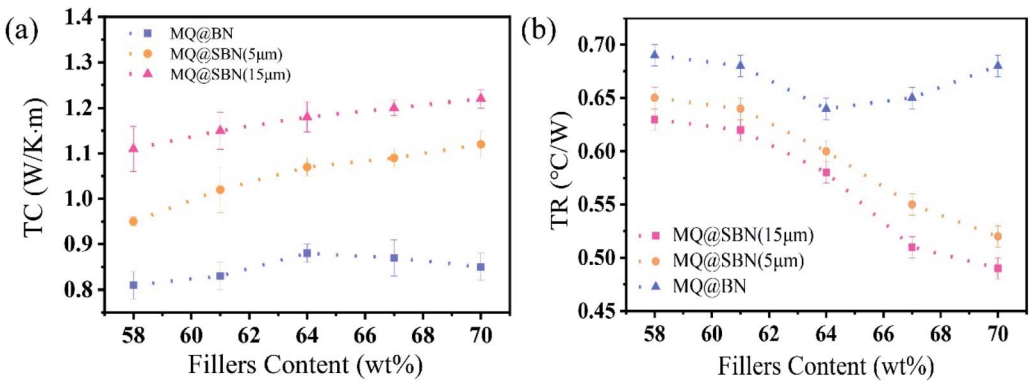

Fig. 8 Effect of filler content on (a) the TC and (b) the TR.

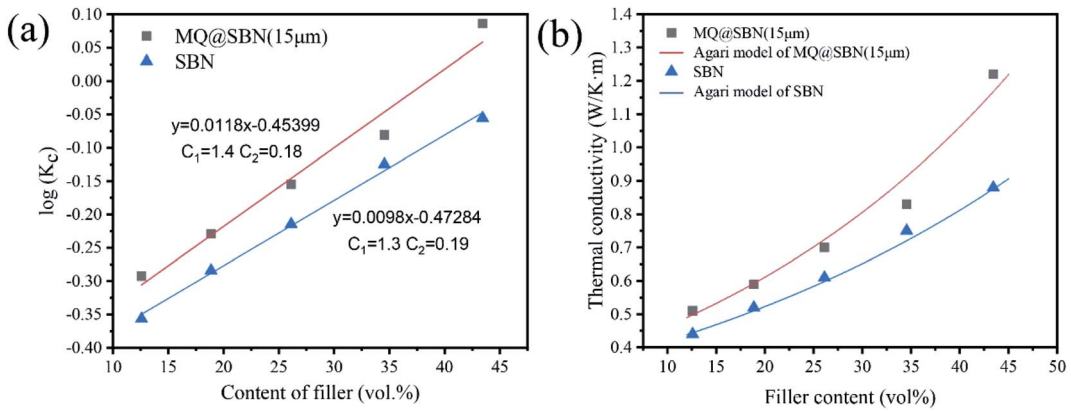

Fig. 9 (a) Logarithm of the TC of SBN/PDMS and MQ@SBN (15 μm)/PDMS linearly fit using Agari's model. (b) Comparison of the measured thermal conductivities of composites with calculated conductivities using Agari's model.

the heat transfer. In the platelet-like MQ@BN/PDMS composites, the contact between the platelets of BN was weak, and the contact area was not sufficient. In contrast, there was no phonon scattering at the interface because of the tight contact in the SBN, thus PDMS could not easily permeate its interior. The interaction between BN and the contact area was extended, which enhanced the TC of the SBN/PDMS composites. The TC of MQ@BN/PDMS also declined when the filler content was greater than 64 wt%. By observing the appearance of HCSG at that point, we found that the MQ@BN/PDMS had hardened owing to the excess filler content of BN, and a defect appeared inside the material. The heat transfer path was destroyed, resulting in a decrease in the TC. Owing to cracks, the grease could not coat the surface of the testing platform, which further increased the TR. On the other hand, SBN showed more contact points, and the weak thickening effect helped maintain the

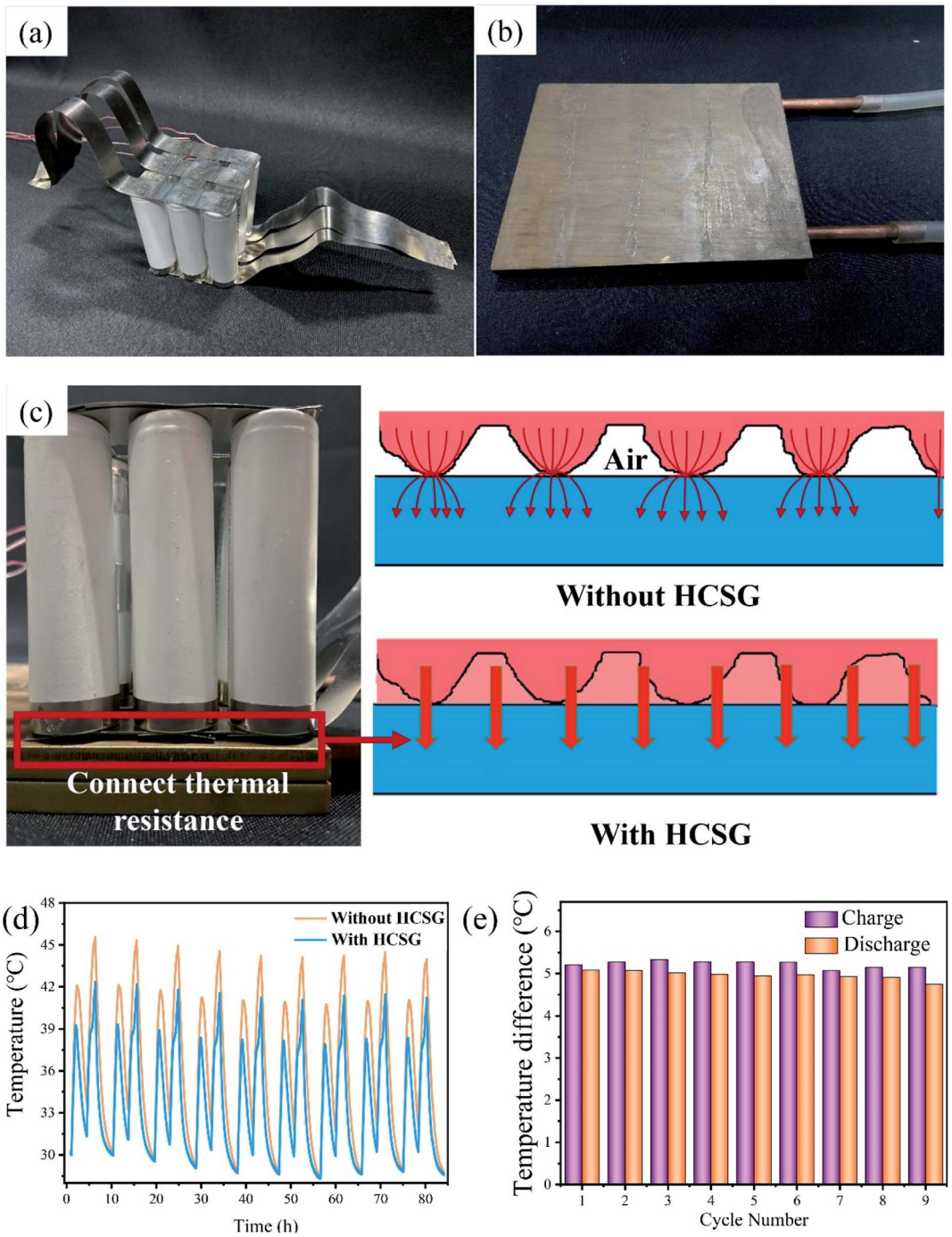

Fig. 10 Photo of (a) the battery module, (b) the liquid-cooling plate, and (c) the testing system. (d) Temperature and (e) temperature difference variations under a cycling test of battery modules with/without HCSG.

HCSG wettability and heat conductivity. The TC values of MQ@SBN(5 μm)/PDMS and MQ@SBN(15 μm)/PDMS were 1.12 and 1.22 W (m^{-1} K^{-1}), respectively, and their TR values were 0.52 and 0.49 °C W^{-1}, respectively. The 15 μm SBN-filled PDMS composites exhibited a higher TC than those filled with 5 μm SBN, probably because the former possesses a superior filler stacking mode.[39,40]

Based on the generalization of models of series and parallel conduction in composites, Agari and Uno[41,42] modified the Maxwell model, and the equation is calculated using the following equation:

$$\log(K_c) = V_f C_2 \log(K_p) + (1 - V_f)\log(C_1 K_m)$$

In which, K_c, K_m, K_p are the thermal conductivity of the polymer composites, the PDMS matrix, and the SBN, respectively. V_f is the volume fraction of the SBN. C_1 is a factor related to the effect of the filler on the secondary structure of the polymer and C_2 is a factor related to the ease of forming conductive chains of filler. Using the data shown in Fig. 9a, It was observed that in our system, the C_1 values of the two composites were higher than 1, indicating that there were no secondary structure effects in the polymer.

3.4 Temperature distribution of the battery modules

The electrochemical performance of LIBs is sensitive to temperature.[43] High temperature conditions can not only result in sharp capacity degradation of LIBs, but also causes some thermal safety problems, including explosion and self-ignition.[44,45] To control the temperature and temperature differences in power battery modules (packs), researchers have developed various battery thermal management system technologies for battery modules.[46] Cylindrical batteries are one of the most common types used in battery modules, which were usually connected in series or parallel using nickel sheets to produce a higher capacity. However, owing to the macroscopic warping of the nickel sheet connected to the batteries, the bottom of the battery module cannot fully contact the liquid-cooling plate.

Therefore, the heat generated by the batteries cannot be transferred to the cooling device in time. TIMs can fill the gap between the module and the liquid-cooling plate to effectively eliminate the air at the interface, increase the heat transfer area, and achieve efficient cooling and temperature uniformity (Fig. 10a–c). As shown in Fig. 10d and e, through analyzing the temperature of the battery module with or without HCSG during the charge and discharge process, it was found that the maximum temperature of the batteries in the module could be maintained below 42 °C during the charging and discharging processes. Compared with that, the maximum temperature of the battery module without HCSG was still almost 45 °C, or even higher. During the entire charge and discharge process, the temperature difference of the module with HCSG could drop to below 5.5 °C, which was obviously lower than that of the module that did not contain HCSG. These results proved that the prepared HCSG materials can satisfy the insulating requirement of batteries, which could expand their application modes.

4 Conclusion

In order to decrease the contact TR, in this study, SBN surfaces constructed using the sedimentation method between MQ and the PDMS matrix have been proposed. A reduced stiffness silica intermediate on the SBN improved the interaction between the stiff SBN and the soft PDMS and reduced the modulus mismatch between them. Heat transfer in the MQ@SBN/PDMS composites was higher than that in the SBN/PDMS composites for 5 and 15 μm SBN loadings with an adequate thickness of MQ. In addition, the spherical-structured filler showed a higher TC than the platelet-like filler. Using a battery liquid-cooling system, the prepared HCSG was proved to meet the insulation requirements and effectively improved the cooling effect. In addition, when the HCSG was assembled on the surface of the liquid-cooling plate in the 18 650-battery module, the maximum temperature of the battery module could be maintained below 42 °C, and the temperature difference can be controlled to within 5 °C. Therefore, it can be concluded that the MQ-modified composite could decrease the TR and improve the installation process, therefore it has great potential for use in fundamental research and advanced applications, such as thermal energy storage and thermal management.

Author contributions

Xin Ge: conceptualization, methodology, investigation, writing – original draft, writing – review and editing, validation. Youpeng Chen: software, data curation. Weidong Liu: resources, supervision. Guoqing Zhang: term, conceptualization, validation, resources, supervision, funding acquisition. Xinxi Li: visualization, writing – review and editing. Jianfang Ge: methodology, writing – review and editing. Canbing Li: supervision, writing – review & editing.

Conflicts of interest

Authors declare that they have no conflict of interest.

Acknowledgements

This work was financially supported by the National Natural Science Foundation of China (NNSFC, 21875046), the Guangzhou Emerging Industry Development Fund Project of Guangzhou Development and Reform Commission (2018841), the Key Fields Special Project of Guangdong Universities (2020ZDZX2076, 2020ZDZX2079), and the Special Funds for Applied Science and Technology Research and Development of Guangdong Province (2015B090925022).

References

1 D. X. Ouyang, J. Liu and M. Chen, An experimental study on the thermal failure propagation in lithium-ion battery pack, *J. Electrochem. Soc.*, 2018, **165**, 2184–2193.

2 Z. X. Zhang, R. Xun, L. J. Wang and Z. H. Meng, Construction of pseudocapacitive Li2-xLaxZnTi3O8 anode for fast and super-stable lithium storage, *Ceram. Int.*, 2021, **47**, 662–669.
3 K. Jiang, G. L. Liao, J. Q. E, F. Zhang, J. W. Chen and E. Leng, Thermal management technology of power lithium-ion batteries based on the phase transition of materials: A review, *Journal of Energy Storage*, 2020, **32**, 101816.
4 Y. Azizi and S. M. Sadrameli, Thermal management of a $LiFePO_4$ battery pack at high temperature environment using a composite of phase change materials and aluminum wire mesh plates, *Energy Convers. Manage.*, 2016, **128**, 294–302.
5 J. Zhang, X. Wu, K. Chen, D. Zhou and M. Song, Experimental and numerical studies on an efficient transient heat transfer model for air-cooled battery thermal management systems, *J. Power Sources*, 2021, **490**, 229539.
6 A. Abdulrahim and J. Chung, Performance improvement of cogeneration plants in hot arid regions via sustainable turbine inlet air cooling technologies: An energy-water nexus comparative case study, *Int. J. Energy Res.*, 2021, **45**, 10765–10793.
7 H. Behi, D. Karimi, M. Behi, M. Ghanbarpour, J. Jaguemont, M. A. Sokkeh, F. H. Gandoman, M. Berecibar and J. Van Mierlo, A new concept of thermal management system in Li-ion battery using air cooling and heat pipe for electric vehicles, *Appl. Therm. Eng.*, 2020, **174**, 115280.
8 L. Sheng, H. Zhang, L. Su, Z. D. Zhang, H. Zhang, K. Li, Y. D. Fang and W. Ye, Effect analysis on thermal profile management of a cylindrical lithium-ion battery utilizing a cellular liquid-cooling jacket, *Energy*, 2020, **220**(1), 119725.
9 S. Chen, X. Wei, A. Garg and L. Gao, A Comprehensive Flowrate Optimization Design for a Novel Air-Liquid-cooling Coupled Battery Thermal Management System, *J. Electrochem. Energy Convers. Storage*, 2020, **18**(2), 021008.
10 Y. Yang, W. Li, X. Xu and G. Y. Tong, Heat dissipation analysis of different flow path for parallel liquid-cooling battery thermal management system, *Int. J. Energy Res.*, 2020, **44**, 5165–5176.
11 X. H. Wu, C. M. Mo, J. K. Xie, X. Q. Yang and G. Q. Zhang, Experimental study of a novel strategy to construct the battery thermal management module by using tubular phase change material units, *Journal of Energy Storage*, 2021, **39**, 102585.
12 H. Gao, M. Chen, J. J. Hong, Y. C. Song and Y. Y. Yan, Investigation on battery thermal management based on phase change energy storage technology, *Heat Mass Transfer*, 2021, **30**(8), 1904228.
13 J. Deng, X. X. Li, G. Q. Zhang, Z. X. Wu, C. B. Li, Q. Q. Huang and C. X. Yang, Flexible Composite Phase-Change Material with Shape Recovery and Antileakage Properties for Battery Thermal Management, *ACS Appl. Energy Mater.*, 2021, **4**(12), 13890–13902.
14 Y. Zheng, Y. Shi and Y. Huang, Optimisation with adiabatic interlayers for liquid-dominated cooling system on fast charging battery packs, *Appl. Therm. Eng.*, 2019, **147**, 636–646.
15 Z. Q. Liu, J. H. Huang, M. Cao, G. W. Jiang, J. Hu and Q. Chen, Preparation of Binary thermal silicone grease and Its application in battery thermal management, *Materials*, 2020, **13**(21), 4763.
16 C. R. Xiao, G. Q. Zhang, Z. H. Li and X. Q. Yang, Custom design of solid-solid phase change material with ultra-high thermal stability for battery thermal management, *J. Mater. Chem. A*, 2020, **8**, 14624.
17 R. V. Gorbachev, R. Ibtsam, R. R. Nair, J. Rashid, B. Liam, B. D. Belle, E. W. Hill, K. S. Novoselov, W. Kenji and T. Takashi, Hunting for monolayer boron nitride: optical and Raman signatures, *Small*, 2015, **7**, 465–468.
18 K. K. Kim, A. Hsu, X. Jia, S. M. Kim, Y. Shi, M. Hofmann, D. Nezich, J. F. Rodriguez-Nieva, M. Dresselhaus and T. Palacios, Synthesis of monolayer hexagonal boron nitride on Cu foil using chemical vapor deposition, *Nano Lett.*, 2012, **12**, 161–166.
19 G. Christensen, D. Lou, H. P. Hong and G. P. Peterson, Improved Thermal Conductivity of Fluids and Composites Using Boron Nitride (BN) Nanoparticles through Hydrogen Bonding, *Thermochim. Acta*, 2021, **700**, 178927.
20 Y. J. Gou, Z. L. Liu, G. M. Zhang and Y. X. Li, Effects of multi-walled carbon nanotubes addition on thermal properties of thermal grease, *Int. J. Heat Mass Transfer*, 2014, **74**, 358–367.
21 J. Zhao, F. Du, C. Wei, Z. Ping, X. Zhou and X. Xie, Effect of silica coating thickness on the thermal conductivity of polyurethane/SiO_2 coated multiwalled carbon nanotube composites, *Composites, Part A*, 2014, **58**, 1–6.
22 C. Wei, F. Du, J. Zhao, Z. Wei, Y. Yang, X. Xie and Y. W. Mai, Improving thermal conductivity while retaining high electrical resistivity of epoxy composites by incorporating silica-coated multi-walled carbon nanotubes, *Carbon*, 2011, **49**, 495–500.
23 K. Ahn, K. Kim and J. Kim, Fabrication of surface-treated BN/ETDS composites for enhanced thermal and mechanical properties, *Ceram. Int.*, 2015, **41**, 9488–9495.
24 K. Kim, K. Ahn, H. Ju and J. Kim, Improvement of Insulating and Thermal Properties of SiO2-Coated Copper Nanowire Composites, *Ind. Eng. Chem. Res.*, 2016, **55**, 2713–2720.
25 L. Ren, X. Zeng, R. Sun, J. Bin Xu and C. P. Wong, Spray-assisted assembled spherical boron nitride as fillers for polymers with enhanced thermally conductivity, *Chem. Eng. J.*, 2019, **370**, 166–175.
26 M. M. Rueda, M.-C. Auscher, R. Fulchiron, T. Périé, G. Martin, P. Sonntag and P. Cassagnau, Rheology and applications of highly filled polymers: A review of current understanding, *Prog. Polym. Sci.*, 2017, **66**, 22–53.
27 H. J. Ahn, Y. J. Eoh, S. D. Park and E. S. Kim, Thermal conductivity of polymer composites with oriented boron nitride, *Thermochim. Acta*, 2014, **590**, 138–144.
28 H. Xiang, J. Ge, S. Cheng, H. Han and S. Cui, Synthesis and characterization of titania/MQ silicone resin hybrid nanocomposite via sol-gel process, *J. Sol-Gel Sci. Technol.*, 2011, **59**, 635–639.
29 Y. Yang, S. Qiu, W. Cui, Q. Zhao, X. Cheng, R. K. Y. Li, X. Xie and Y.-W. Mai, A facile method to fabricate silica-coated

carbon nanotubes and silica nanotubes from carbon nanotubes templates, *J. Mater. Sci.*, 2009, **44**, 4539–4545.

30 Y. W. Mai and Z.-Z. Yu, *Polymer nanocomposites*, Woodhead publishing, 2006.

31 D. G. Cahill, P. V Braun, C. Gang, D. R. Clarke, S. Fan, K. E. Goodson, P. Keblinski, W. P. King, G. D. Mahan and A. Majumdar, Nanoscale thermal transport. II. 2003-2012, *Appl. Phys. Rev.*, 2014, **1**, 251–265.

32 H. Ming, P. Keblinski and P. K. Schelling, Kapitza conductance of silicon-amorphous polyethylene interfaces by molecular dynamics simulations, *Phys. Rev. B: Condens. Matter Mater. Phys.*, 2009, **79**, 104305.

33 H. Ming, S. Shenogin and P. Keblinski, Molecular dynamics simulation of interfacial thermal conductance between silicon and amorphous polyethylene, *Appl. Phys. Lett.*, 2007, **91**, 241910.

34 J. E. Peters, D. V Papavassiliou and B. P. Grady, Unique Thermal Conductivity Behavior of Single-Walled Carbon Nanotube−Polystyrene Composites, *Macromolecules*, 2012, **41**, 7274–7277.

35 Y. K. Kim, J. Y. Chung, J. G. Lee, Y. K. Baek and P. W. Shin, Synergistic effect of spherical Al2O3 particles and BN nanoplates on the thermal transport properties of polymer composites, *Composites, Part A*, 2017, **98**, 184.

36 S. T. Huxtable, D. G. Cahill, S. Sergei, X. Liping, O. Rahmi, B. Paul, U. Monica, M. S. Strano, S. Giles and S. Moonsub, Interfacial heat flow in carbon nanotube suspensions, *Nat. Mater.*, 2003, **2**, 731–734.

37 S. Y. Yang, C. C. M. Ma, C. C. Teng, Y. W. Huang, S. H. Liao, Y. L. Huang, H. W. Tien, T. M. Lee and K. C. Chiou, Effect of functionalized carbon nanotubes on the thermal conductivity of epoxy composites, *Carbon*, 2010, **48**, 592–603.

38 L. Chen, H. F. Xu, S. J. He, Y. H. Du, N. J. Yu, X. Z. Du, J. Lin and S. Nazarenko, Thermal Conductivity Performance of Polypropylene Composites Filled with Polydopamine-Functionalized Hexagonal Boron Nitride, *PLoS One*, 2017, **12**, e0170523.

39 B. L. Zhu, J. Ma, J. Wu, K. C. Yung and C. S. Xie, Study on the Properties of the Epoxy-Matrix Composites Filled with Thermally Conductive AlN and BN Ceramic Particles, *J. Appl. Polym. Sci.*, 2010, **118**, 2754–2764.

40 K. C. Yung and H. Liem, Enhanced Thermal Conductivity of Boron Nitride Epoxy-Matrix Composite Through Multi-Modal Particle Size Mixing, *J. Appl. Polym. Sci.*, 2010, **106**, 3587–3591.

41 Y. Agari and T. Uno, Thermal conductivity of polymer filled with carbon materials: effect of conductive particle chains on thermal conductivity, *J. Appl. Polym. Sci.*, 1985, **30**, 2225–2235.

42 Y. Agari, M. Tanaka, S. Nagai and T. Uno, Thermal conductivity of a polymer composite filled with mixtures of particles, *J. Appl. Polym. Sci.*, 1987, **34**, 1429–1437.

43 H. Q. Liu, Z. B. Wei, W. D. He and J. Y. Zhao, Thermal issues about Li-ion batteries and recent progress in battery thermal management systems: A review, *Energy Convers. Manage.*, 2017, **150**, 304–330.

44 T. R. Ashwin, Y. M. Chung and J. H. Wang, Capacity fade modelling of lithium-ion battery under cyclic loading conditions, *J. Power Sources*, 2016, **328**, 586–598.

45 X. H. Liu, W. L. Ai, M. N. Marlow, Y. Patel and B. Wu, The effect of cell-to-cell variations and thermal gradients on the performance and degradation of lithium-ion battery packs, *Appl. Energy*, 2019, **248**, 489–499.

46 S. Arora, Selection of thermal management system for modular battery packs of electric vehicles: A review of existing and emerging technologies, *J. Power Sources*, 2018, **400**, 621–640.